CHEMISTRY OF MATERIALS

pubs.acs.org/cm

Article

From Well-Defined Clusters to Functional Materials: Molecular Engineering of Amorphous Molybdenum Sulfides for Hydrogen Evolution Electrocatalysis

Published as part of the Chemistry of Materials virtual special issue "In Honor of Prof. Clement Sanchez".

Francisco Gonell, Miriam Rodenes, Santiago Martín, Mercedes Boronat, Iván Sorribes,* and Avelino Corma*

Cite This: *Chem. Mater.* 2023, 35, 8483−8493

Read Online

ACCESS | Metrics & More | Article Recommendations | Supporting Information

ABSTRACT: Developing precious-metal-free electrocatalysts for the hydrogen evolution reaction (HER) is crucial to establishing H_2 produced from renewable energy sources as an alternative energy carrier to fossil fuels. Amorphous molybdenum sulfide-based materials are promising candidates that provide highly active HER electrocatalysts by introducing active sites at both the edge positions and the typically inactive basal planes. Herein, we report an innovative bottom-up synthesis of amorphous molybdenum sulfides using molecular complexes with Mo_3S_4 and Mo_3S_7 cluster cores as building entities. The ability to control the precursor of choice has made it viable to enhance the HER activity of these materials. Furthermore, the tunability of the atomic composition of the molecular cluster precursors allows the modification of the derived materials with atomic-scale precision, enabling us to track the synthesis mechanism and, in combination with Density Functional Theory (DFT) calculations, to decipher the nature of the HER active sites.

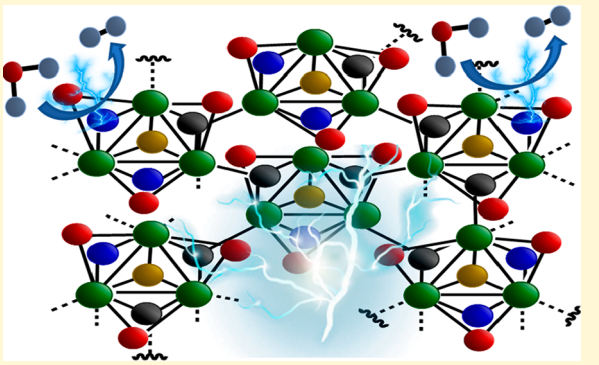

INTRODUCTION

The global energy scenario urges the development of more sustainable energy production sources able to substitute for finite fossil fuels and reduce global carbon dioxide (CO_2) emissions. In recent decades, technologies able to take profit from renewable energy sources, such as solar and wind, are showing a remarkable maturity. However, the intrinsic intermittency of these renewable energies makes necessary their conversion into energy carriers for long-term storage in order to use them on-demand for off-grid applications. In this context, water electrolysis has drawn enormous attention as a convenient energy-harvesting technology because it allows the storage of renewable electricity in hydrogen (H_2), which is considered the most promising alternative energy carrier for fossil fuels.[1,2]

The hydrogen evolution reaction (HER), in which protons from water are reduced to H_2, is thermodynamically feasible, but the use of a highly efficient catalyst is required to drive the HER at low overpotentials and high reaction rates. Platinum-based materials are the most efficient HER electrocatalysts to date; however, the scarcity and high cost of this metal greatly hamper the large-scale application of this technology to realize a sustainable energetic scheme based on the so-called "hydrogen economy".[3−6] Thus, finding nonprecious HER electrocatalysts is of the utmost importance.

Early studies on bulk molybdenum disulfide (MoS_2) indicated that this inorganic material displayed modest activity for HER.[7,8] Nevertheless, since pioneering theoretical and experimental investigations revealed that the edges of MoS_2 can act as active sites for this electrocatalytic reaction,[9,10] molybdenum sulfides have emerged as promising materials in the quest of cost-effective and scalable HER electrocatalysts under acidic conditions. With the aim of increasing the HER performance of molybdenum sulfides, much effort has been devoted on developing synthetic strategies in order to maximally expose the active edge sites, for example, by nanostructuring these materials (in the form of nanoparticles,[10] nanosheets,[11] or nanowires[12]), by material exfoliation, thin film deposition,[13,14] or preparation of nanocomposites with

Received: May 23, 2023
Revised: September 18, 2023
Published: October 16, 2023

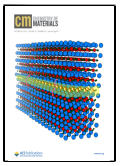

conductive supports.[15−17] However, the HER activity of these materials mainly originates from the edge sites, whereas basal planes are catalytically inert. Therefore, considering the small perimeter-to-basal plane area ratio, characteristic of this type of material, most promising approaches to improve their intrinsic activity must involve the activation of the basal planes by disorder engineering, i.e., by introducing structural defects.[18] Among others, post-treatment of the basal surface by H_2 annealing,[19−21] plasma bombardment,[22,23] irradiation treatment,[24,25] wet chemical etching,[26,27] electrochemical activation,[28,29] elemental doping,[30,31] or phase transition engineering[32,33] are some of the strategies applied for this purpose. In particular, the isolation of the 1T-MoS_2 phase displaying metallic character is worth mentioning because of its excellent catalytic activity, which is ascribed to the larger electron mobility and the proliferated active sites in both the basal plane and edges.[34−36] Unfortunately, the 1T phase is thermodynamically unstable and gradually converts into the semiconducting 2H phase.[37]

Furthermore, the preparation of amorphous molybdenum sulfides is a convenient strategy to promote the HER activity of these kinds of materials. Typical preparation methodologies of amorphous molybdenum sulfides involve electrodeposition[38−43] or wet chemical synthesis,[44,45] which renders materials with high surface area, enhanced roughness, and a number of defects at both the edge positions and basal planes. However, reported studies on the identification of the nature of the electrocatalytic active sites of these catalysts vary widely and even conflict with each other, likely because of the atomic-scale heterogeneity, which arises from the lack of control during the synthetic process.[39−43,46,47]

It is generally accepted that the structure of amorphous molybdenum sulfides is constituted by polymeric aggregations of trimeric Mo^{IV} cluster units displaying different kinds of sulfide ligands.[41−43] Interestingly, well-known molecular complexes with cluster cores $Mo_3(\mu_3\text{-}S)(\mu\text{-}S_{ax})_3$, $Mo_3(\mu_3\text{-}S)(\mu\text{-}S_{ax}\text{-}S_{eq})_3$, and $Mo_3(\mu_3\text{-}S)(\mu\text{-}S_{ax}\text{-}S_{eq})_3(S_2)_3$ (hereinafter named Mo_3S_4, Mo_3S_7, and Mo_3S_{13}, respectively) feature similar topologies to those found in amorphous molybdenum sulfide (Scheme 1).

Scheme 1. Molecular Complexes Displaying (a) Mo_3S_4, (b) Mo_3S_7, and (c) Mo_3S_{13} Cluster Cores and (d) Schematic Representation of Amorphous Molybdenum Sulfide[41−43]

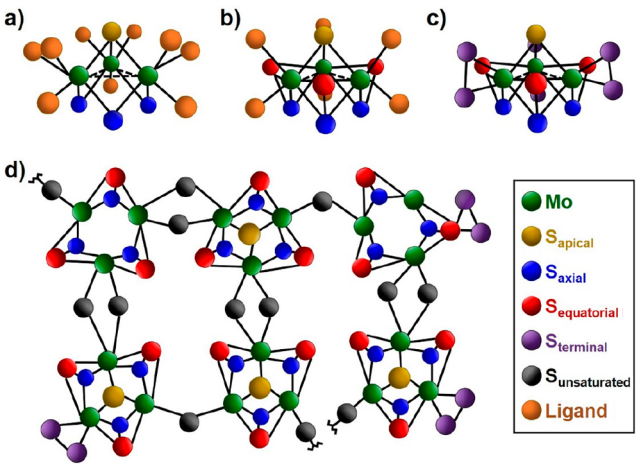

These kind of trimeric cluster complexes are air-stable and can be readily prepared by scaled methods, a fact that has boosted their use to prepare HER catalysts for electrocatalytic[48−52] and light-driven[53−58] water splitting. In the context of the electrocatalytic HER, Chorkendorff and co-workers were pioneers in depositing an incomplete cubane-type $[Mo_3S_4]^{4+}$ cluster on different graphite supports (high surface carbon, Vulcan XC72, and highly oriented pyrolytic graphite, HOPG) and applied them as novel prototype catalysts in heterogeneous catalysis for this reaction.[48] In 2014, Besenbacher and co-workers reported more active and stable catalysts prepared by depositing a thiomolybdate $[Mo_3S_{13}]^{2-}$ cluster on HPOG and graphite paper (GP) of high surface area. The origin of the high activity was ascribed to the different sulfur species, all of them inherently exposed and thus considered as active edge sites.[49,50] Some years later, the thiomolybdate $[Mo_3S_{13}]^{2-}$ cluster was anchored on highly conductive reduced graphene oxide-carbon nanotubes (rGO/CNTs) aerogels, a fact that resulted in the beneficial suppressing of the aggregation of the cluster complex, exposing more active sulfur sites, and enhancing electron diffusion.[49,50] The thiomolybdate $[Mo_3S_{13}]^{2-}$ cluster was also used to prepare electrodeposited Mo_3S_{13} films, which exhibited highly efficient electrocatalytic activity for HER. The good conductivity and the presence of a high degree of disulfide bridging S_2^{2-} and apical S^{2-} (blue/red and yellow spheres in Scheme 1c, respectively) species were proposed to be the responsibility of the high HER activity.[52] Yaghi's group synthesized dimers and chains comprising Mo_3S_7 cluster units connected with organic linkers, which resulted in more efficient HER electrocatalysts than discrete $[Mo_3S_7Br_6]^{2-}$ and $[Mo_3S_{13}]^{2-}$ complexes, shown in Scheme 1b,c, respectively.[51] Later, recent studies reported the preparation of a $[Mo_3S_{13}]^{2-}$-derived MoS_x catalyst; however, its HER activity was lower than that of a catalyst constituted by polymeric chains comprising monomeric S^{2-} instead of disulfide bridging S_2^{2-} sites.[59]

In this work, amorphous molybdenum sulfides have been engineered with high control at the atomic scale through an innovative bottom-up synthetic strategy based on the use of molecular complexes with Mo_3S_4 and Mo_3S_7 cluster cores as building entities (Scheme 1a,b, respectively).[60] This synthetic strategy is particularly advantageous because it allows introducing well-defined modifications into the final amorphous materials through exquisite control of the atomic positions of the cluster entities. Derived from their extended-molecular nature and their processability in the form of a heterojunction with conductive carbon materials, highly active HER electrocatalysts are obtained. The rational design of amorphous materials with atomic-scale precision in combination with Density Functional Theory (DFT) calculations has allowed us to decipher the nature of the active sites involved in the HER.

EXPERIMENTAL SECTION

Synthesis. Reagents were obtained from commercial sources and used as received. In general, since selenium is toxic, special care was taken when preparing molecular complexes containing this element. The molecular cluster precursors $[Mo_3S_7Cl_6](n\text{-}Bu_4N)_2$[61] and $[Mo_3S_4Se_3Cl_6](n\text{-}Bu_4N)_2$[62] were prepared according to literature methods.

The complexes $[Mo_3Se_7Br_6](PPh_4)_2$ and $[Mo_3SSe_6Br_6](PPh_4)_2$ were prepared from the corresponding polymers $\{Mo_3Se_7Br_4\}_n$[63,64] and $\{Mo_3SSe_6Br_4\}_n$,[65] respectively, following a slightly modified

https://doi.org/10.1021/acs.chemmater.3c01260
Chem. Mater. 2023, 35, 8483−8493

procedure with respect to the ones previously reported.[63,64] Briefly, the polymer (1 g) and PPh_4Br (2 g) were melted in a vacuum-sealed quartz ampule at 310 °C (rate 5 °C/min) for 3 h. Then, the ampule was cooled down to room temperature and opened. The obtained solid was washed with plenty ethanol, extracted with acetonitrile, and filtered. Finally, the red colored solution was evaporated under vacuum to obtain the desired complex.

The complex $Mo_3S_4(PPh_3)_3Cl_4(MeOH)_2$ was prepared as previously reported.[60] The same strategy was applied to synthesize the bromide analogue displaying Se at the axial positions "Mo_3SSe_3". Accordingly, $[Mo_3SSe_6Br_6](PPh_4)_2$ (1 g) was dissolved with methanol (25 mL) under nitrogen in a 50 mL Schlenk flask containing a stirring bar. Then, triphenylphosphine (13.4 equiv, 1.8 g) was added, producing a color change from dark red to brown. The mixture was stirred overnight at room temperature and filtered under vacuum, and the recovered solid was washed using a mixture of cold *n*-hexane:toluene (1:1) and then with hot *n*-hexane. The obtained brown solid was allowed to dry under ambient conditions.

$[Mo_3SSe_3S_3Br_6](n\text{-}Bu_4N)_2$ was prepared through a two-steps synthesis. In the first one, the molecular complex "Mo_3SSe_3" experiences sulfurization and coordination by disphosphate ligands $(EtO)_2PS_2^-$ (dtp), as previously reported for structure related clusters.[66] For that, a freshly prepared solution of P_4S_{10} (5.881 g) in ethanol (28 mL) was added to a suspension of "Mo_3SSe_3" (1 g) in ethanol (150 mL) under nitrogen, and the mixture was stirred for 24 h. After this time, the mixture was filtered under a vacuum, and the recovered solid was washed with acetonitrile, ethanol, and diethyl ether. Finally, the orange solid, mainly composed of the complex $[Mo_3Se_4S_3((EtO)_2PS_2)_3]Br$ (Figure SI1), was allowed to dry under ambient conditions. In a second step, the obtained molecular complex was refluxed overnight in a mixture of acetonitrile (270 mL) and aqueous HBr (48%, 55 mL). Formation of a copious white solid was formed, which was separated from the orange solution by filtration. Next, the filtrate was taken to dryness under a vacuum and redissolved with the minimum amount of hot aqueous HBr (48%). After cooling down to room temperature, $(n\text{-}Bu_4N)Br$ was added until complete precipitation of an orange-brown solid. Finally, the solid was recovered by filtration under vacuum and washed with water, ethanol, and diethyl ether.

General Procedure for the Synthesis of Nanomaterials $\{Mo_3Q_{4-7}\}_n$ *(Q = S, Se).* The molecular complexes (0.1563 mmol; 189.1 mg of $[Mo_3S_7Cl_6](n\text{-}Bu_4N)_2$, 210.9 mg of $[Mo_3S_4Se_3Cl_6](n\text{-}Bu_4N)_2$, 305.1 mg of $[Mo_3SSe_6Br_6](PPh_4)_2$, 252.7 mg of $[Mo_3SSe_3S_3Br_6](n\text{-}Bu_4N)_2$, 312.4 mg of $[Mo_3Se_7Br_6](PPh_4)_2$, 215.8 mg of $Mo_3S_4(PPh_3)_3Cl_4(MeOH)_2$, 265.6 mg of "$Mo_3SSe_3$") and carbon powder (VULCAN XC72R, 150 mg (30 wt % Mo, see Supporting Information for further details, Figure SI2)) were dispersed in distilled water (50 mL) into a 100 mL flask containing a stirring bar. While the dispersion was stirred at room temperature, hydrazine monohydrate (64−65%, 10 mL) was slowly added. After 3 h, the mixture was filtered under a vacuum, and the recovered solid was washed with water, ethanol, acetone, and diethyl ether. Finally, the obtained black powder was allowed to dry under ambient conditions and stored under a nitrogen atmosphere.

The series of nanomaterials $\{Mo_3S_{4-7}\}_n$, with several cluster molar compositions (0, 25, 50, 75, 100%), were prepared according to the above procedure by combining different amounts of the molecular complexes $Mo_3S_4(PPh_3)_3Cl_4(MeOH)_2$ (215.8, 161.9, 107.9, 54.0, 0.0 mg, respectively) and $[Mo_3S_7Cl_6](n\text{-}Bu_4N)_2$ (0.0, 47.3, 94.6, 141.8, 189.1 mg, respectively), which were ground together in a previous step.

It should be noted that all nanomaterials $\{Mo_3Q_{4-7}\}_n$ (Q = S, Se) were prepared in the absence of a carbon support for characterization experiments.

Characterization. XRD analyses were carried out with a PANalytical Cubix'Pro diffractometer equipped with an X'Celerator detector and automatic divergence and reception slits using Cu Kα radiation (0.154056 nm).

X-ray photoelectron spectra were acquired with a monochromatic Al Kα X-ray source (1486.6 eV) using a pass energy of 20 eV and a photoelectron take off angle of 90° with respect to the sample plane on a Kratos AXIS Ultra DLD spectrometer. The C 1s peak at 285.0 eV was used to provide a precise energy calibration. Spectra treatment was performed using the CASA software.

The Raman spectra were obtained from solid samples by using an excitation wavelength of 514 nm in a Renishaw Raman spectrometer equipped with an Olympus microscope and a CCD detector. The laser power on the sample was ∼1.25 mW and a total of 15 acquisitions were taken for each spectra.

The molybdenum content in the catalysts was determined by inductively coupled plasma with an optical emission spectrometer (ICP-OES) in a Varian 700-ES Series, after complete dissolution of the solids (ca. 20 mg) in a HNO_3/HF/HCl solution (1/1/3 volume ratio). The sulfur content in catalyst was determined by elemental analysis using a Carlo Erba 1106 analyzer.

Samples for TEM were ultrasonically dispersed in CH_2Cl_2 and transferred into carbon-coated copper grids. TEM micrographs were recorded by using a JEOL JEM2100F microscope operating at 200 kV in a transmission (TEM) mode.

Reaction Conditions. *Electrochemical Characterization.* The electrocatalytic properties were studied through a three-electrode setup, using a glassy carbon (5 mm diameter) rotating disk electrode (RDE, Autolab), glassy carbon rod, and Ag/AgCl electrodes as a working, counter, and reference electrodes, respectively, connected to an AUTM204.S AutoLab potentiostat. The Ag/AgCl electrode was calibrated by using a reversible hydrogen RE (HydroFlex, from Gaskatel, Germany). The potentials were corrected for the *iR* drop by measuring the electrolyte resistance through high-frequency AC impedance.

A conductive ink was prepared by sonicating the electrocatalyst (12 mg) in 1.9 mL of tetrahydrofuran for 30 min. A total of 100 μL of Nafion solution (5 wt %) was added, and the suspension was sonicated during 5 min. A total of 10 μL of the ink was loaded on the RDE previously polished and left to dry, and this process was repeated until the desired catalyst loading. The film was dried for 30 min and then hydrated with one drop of the electrolyte during 5 min before the experiments. All the measurements were performed in 0.5 M H_2SO_4 electrolyte saturated in N_2 at a 10 mV s^{-1} scan rate and a rotation rate of 1600 rpm. Stability tests were performed in the same configuration by cycling between −0.1 and −0.25 V vs RHE at a scan rate of 50 mV s^{-1}.

TOF calculation was performed following the methodology described by Jaramillo and co-workers through the calculation of the capacitance of the materials in the non-Faradaic region.[44]

The electrochemical properties were assessed in a 0.1 M $[Bu_4N]PF_6$ solution in acetonitrile under N_2 atmosphere and in static conditions. The three electrode configuration consisted of a glassy carbon (5 mm diameter), Pt wire, and Ag/Ag^+ (CHI, electrode filled with the same electrolyte solution with 0.01 M of $AgNO_3$) as the working, counter, and reference electrodes, respectively. A total of 10 μL of the ink (10 mg of $\{Mo_3S_4\}_n$ or $\{Mo_3S_7\}_n$, without carbon support, in 2 mL of THF, sonicated for 30 min) were deposited on the glassy carbon electrode and left to dry, to study the electrochemical properties of the materials. The potentials were referenced against ferrocene oxidation/reduction waves.

Computational Details. All calculations are based on density functional theory (DFT) and were performed with the Gaussian09 software[67] using the hybrid B3LYP functional,[68,69] the standard 6-311g(d,p) basis set[70,71] for S, Se, O, and H atoms and the effective core potential LANL2DZ basis set for Mo atoms.[72,73] In all cases, the positions of all atoms in the system were fully optimized without any restriction. All stationary points were characterized by means of harmonic frequency calculations, which also provided thermal corrections to calculate Gibbs free energies under standard state conditions. Atomic charges were calculated using the natural bond order (NBO) approach.[74]

https://doi.org/10.1021/acs.chemmater.3c01260
Chem. Mater. 2023, 35, 8483−8493

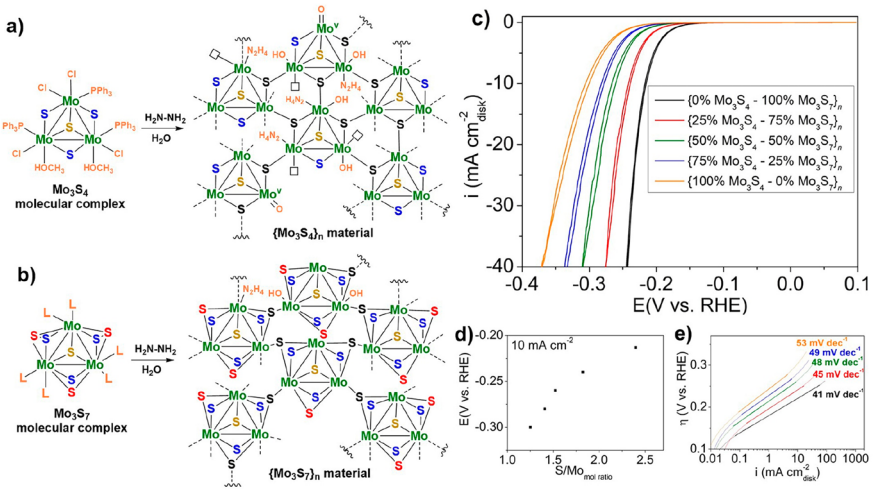

Figure 1. (a) Synthesis of $\{Mo_3S_4\}_n$ and (b) $\{Mo_3S_7\}_n$ from molecular cluster complexes. (c) CVs in acidic HER conditions of the nanomaterials prepared with several Mo_3S_4−Mo_3S_7 ratios. (d) Potential required to reach 10 mA cm^{-2} versus S/Mo molar ratio of each nanomaterial. (e) Tafel slopes of the nanomaterials. Catalyst loading: 0.31 mg cm^{-2}.

RESULTS AND DISCUSSION

Recently, we previously described the preparation of a sulfur deficient MoS_2-type nanomaterial, named $\{Mo_3S_4\}_n$, which was engineered from a Mo_3S_4 cluster complex (Figure 1a). In this synthesis, the molecular cluster, composed by three metal atoms defining an equilateral triangle, an apical sulfur atom (Mo_3-μ_3-S), and three bridging sulfur ligands (Mo_2-μ-S), is reduced with hydrazine hydrate, thereby enabling the intercluster self-assembly by nucleophilic attack from the bridging sulfur ligands to the outer coordination sites of Mo atoms.[60] Remarkably, the peculiar structure configuration of these subunits enabled an advanced heterogeneous hydrogenation and dehydrogenation catalyst to be obtained[60,75] that displays proliferated structural defects on both the naturally occurring edge positions and along the typically inactive basal planes.

The polarization curves in HER for $\{Mo_3S_4\}_n$ revealed discrete activity, with a potential of −0.3 V vs RHE being necessary to reach a current density of 10 mA/cm^2 (Figure 1c). Previous works dealing with amorphous molybdenum sulfide have proposed the sulfur species as the active sites where protons (H^+) from the solution are captured and reduced to H_2 by electrons.[39,40,42,43,46,47] Based on this consideration, we envisioned that the use of molecular cluster entities with a higher population of bridging sulfur ligands could generate amorphous molybdenum sulfide nanomaterials with enhanced HER activity. To check this hypothesis, we tuned our previously reported synthetic methodology by combining molecular complexes with Mo_3S_4 and Mo_3S_7 cluster cores with the aim to precisely modulate the population of the active sites in the prepared nanomaterials. Both molecular cluster entities display a similar structural arrangement, the only difference between them being the nature of the bridging sulfur ligands, which are monatomic in Mo_3S_4 but diatomic in Mo_3S_7 (Scheme 1). The presence of the S−S bridge in the molecular Mo_3S_7 cluster is reflected in the corresponding Raman spectrum with a band centered at 560 cm^{-1} (Figure SI3). However, this Raman vibration band is absent in the spectra of the nanomaterials prepared from the Mo_3S_7 molecular complex. This suggests that upon addition of hydrazine hydrate in the nanomaterial preparation, the starting saturated S−S bridges are reduced and evolve to coordinatively unsaturated sulfur species (Mo_2-μ-S), similar to those present in the Mo_3S_4 precursor. The nucleophilic attack of this unsaturated sulfur species to the outer coordination sites of Mo atoms promotes cluster self-assembly and, hence, the formation of $\{Mo_3S_{4-7}\}_n$ nanomaterials (Figure 1b). Additionally, all nanomaterials exhibit the Raman vibration bands characteristic of the trimetallic sulfide units, including those from metallic bonds (ν(Mo−Mo)) at 125−230 cm^{-1}, molybdenum sulfide bonds (ν(Mo−S)) at 240−384 cm^{-1}, bridging sulfur ligands (ν(μ-S−Mo)) at 430 cm^{-1}, and the apical sulfur atom (ν(μ_3-S−Mo)) at 448 cm^{-1} (Figure SI3).[41,42]

The X-ray diffraction (XRD) patterns of $\{Mo_3S_{4-7}\}_n$ nanomaterials show broad diffraction peaks like those previously found in the $\{Mo_3S_4\}_n$ counterpart, resembling the XRD pattern of the poor crystalline hexagonal structure of MoS_2 (Figure SI4).[76] The amorphous nature of these nanomaterials is also supported by the lack of lattice or Moiré fringes in the bright field transmission electron microscopy (TEM) images (Figure SI5). High-resolution S 2p core-level spectra obtained by X-ray photoelectron spectroscopy (XPS) of the series of $\{Mo_3S_{4-7}\}_n$ nanomaterials could be fitted into two sets of doublets, characteristic of the spin−orbit splitting of S $2p_{3/2}$ and S $2p_{1/2}$ orbitals (Figure SI6). The double peak associated with the unsaturated bridging sulfur ligands (Mo_2-μ-S; blue and red in Figure 1) is located at binding energies (BEs) of 161.9/163.0 eV, whereas the one centered at 162.5/163.7 eV corresponds to the apical sulfur ligands (Mo_3-μ_3-S) and to the saturated sulfurs linking different cluster units (Mo_2-μ-S-Mo; yellow and black color in Figure 1, respectively). The high-resolution Mo 3d XPS core-level spectra showed, after deconvolution and fitting, two sets of doublets, each of them characteristic of the spin−orbit splitting of the Mo $3d_{5/2}$ and Mo $3d_{3/2}$ orbitals. One of these doubles is characteristic of Mo^{IV} species and the other one is ascribed to the presence of molybdenum oxysulfides ($Mo^vO_xS_y$).[41,60,75]

A further evidence of the similar composition, i.e., the presence of the same type of species, in the series of nanomaterials $\{Mo_3S_{4-7}\}_n$ was obtained by comparing their

https://doi.org/10.1021/acs.chemmater.3c01260
Chem. Mater. 2023, 35, 8483−8493

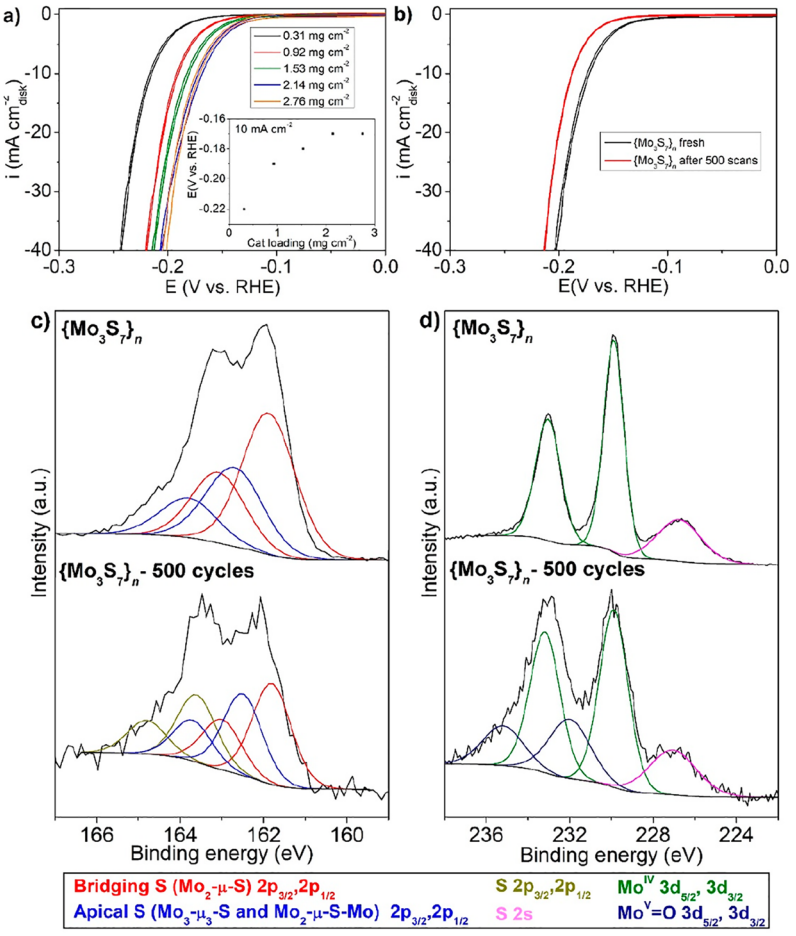

Figure 2. (a) CVs of $\{Mo_3S_7\}_n$ with several loadings. Inset shows the potential required to reach 10 mA cm^{-2} current of each catalyst loading. (b) CVs of $\{Mo_3S_7\}_n$ (loading 2.14 mg cm^{-2}) in 0.5 M H_2SO_4, black line pristine material and red line after 500 scans. S 2p (c) and Mo 3d (d) XPS spectra of pristine $\{Mo_3S_7\}_n$ and after 500 scans.

electrochemical behavior. Cyclic voltammetry (CV) experiments reveal that the molecular Mo_3S_4 and Mo_3S_7 complexes exhibit different redox chemistry (Figure SI7a). However, the CVs of the respective materials show similar profiles with a quasi-reversible reduction wave centered at −0.01 V vs Fc^+/Fc and an irreversible one at −1.25 vs Fc^+/Fc (Figure SI7b). This suggests that, despite the difference in the cluster composition used for their preparation, the redox processes occurring in the nanomaterials are of the same nature.

Gratifyingly, the polarization curves in acidic HER conditions of the nanomaterials $\{Mo_3S_{4-7}\}_n$ prepared from several ratios of both molecular clusters show how the higher the Mo_3S_7 content the higher the HER activity (Figure 1c). A direct correlation is observed between the electrocatalytic activity and the sulfur/molybdenum (S/Mo) ratio (Figure 1d), fully suggesting that the HER active sites increase with the sulfur content of nanomaterials $\{Mo_3S_{4-7}\}_n$. $\{Mo_3S_7\}_n$ shows a Tafel slope of 41 mV dec^{-1}, comparable with other molybdenum sulfides.[15,42,43,77] The increase of the amount of Mo_3S_4 in the synthesis increases the Tafel slope with a maximum value of 53 mV dec^{-1} for $\{Mo_3S_4\}_n$ (Figure 1e), which is consistent with slower kinetics. The HER mechanism in acidic media consists of three possible steps. With a first proton discharge (Volmer step) followed by an electrochemical desorption (Heyrovsky step) or a recombination (Tafel step):[15,77]

$$H^+ + e^- \rightarrow H_{ads} \quad \text{Volmer step (120 mV dec}^{-1}\text{)}$$

$$H_{ads} + H^+ + e^- \rightarrow H_2 \quad \text{Heyrovsky step (40 mV dec}^{-1}\text{)}$$

$$H_{ads} + H_{ads} \rightarrow H_2 \quad \text{Tafel step (30 mV dec}^{-1}\text{)}$$

Although the correlation between the Tafel slope and HER mechanism was developed for metal surfaces, Tafel analysis can give information about the rate-limiting steps during this reaction.[31,77] Pt-based materials show a Tafel slope of 30 mV dec^{-1} indicating that the reaction goes through a Volmer−Tafel mechanism, where the rate-limiting step is the H_{ads} recombination (Tafel step), which is typical of materials with high H_{ads} coverage. In general, lower coverage values promote the HER going through a Volmer-Heyrovsky mechanism with the H_{ads} and H^+ recombination as a rate-limiting step. This is the case of the $\{Mo_3S_7\}_n$ nanomaterial with a Tafel slope of 41 mV dec^{-1}.[15] The same rate-limiting step may dominate in the materials prepared with Mo_3S_4, but the increase in the Tafel slope when the amount of this cluster is increased indicates slower kinetics and hence a decrease in the HER activity.

Further comparison between the $\{Mo_3S_4\}_n$ and $\{Mo_3S_7\}_n$ nanomaterials was investigated by electrochemical impedance spectroscopy (Figure SI8). The fluent charge transport shows

https://doi.org/10.1021/acs.chemmater.3c01260
Chem. Mater. 2023, 35, 8483−8493

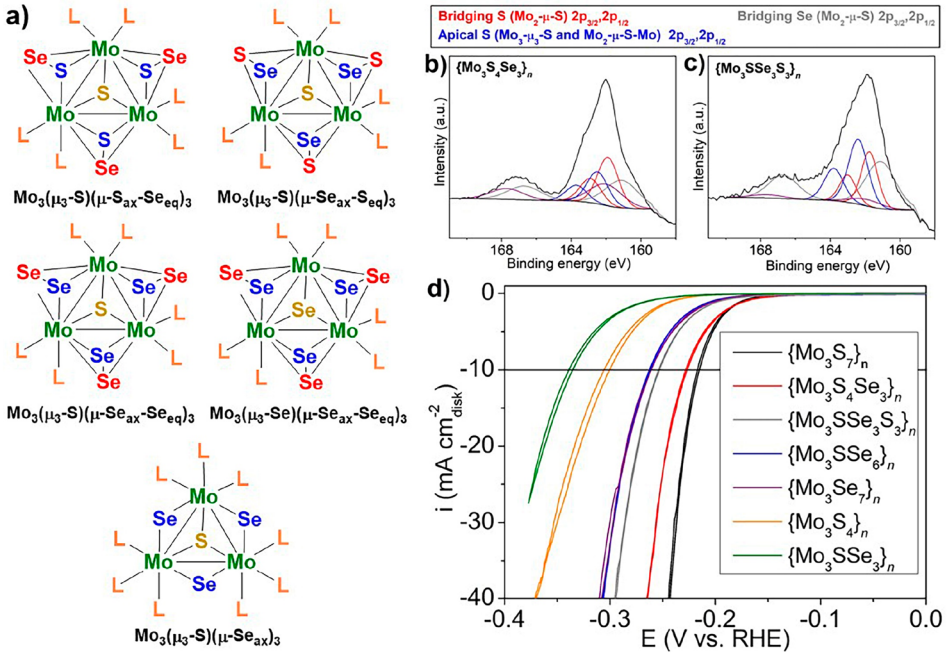

Figure 3. (a) Cluster cores of complexes used as precursors for the preparation of $\{Mo_3Q_{4-7}\}_n$ (Q = S or Se) nanomaterials. S 2p XPS spectra of the nanomaterials (b) $\{Mo_3S_4Se_3\}_n$ and (c) $\{Mo_3SSe_3S_3\}_n$. (d) CVs of $\{Mo_3S_7\}_n$ and $\{Mo_3Q_{7-4}\}_n$ (Q = S, Se) nanomaterials.

that $\{Mo_3S_7\}_n$ has lower charge transfer resistance (~115 Ω) compared to $\{Mo_3S_4\}_n$ (~2000 Ω), which indicates faster electron-transfer kinetics at the electrode/electrolyte interface in $\{Mo_3S_7\}_n$, thus allowing better electron percolation and, hence, higher HER activity.

Additionally, the intrinsic per-site activity is also a good metric to compare the efficiency of catalysts. The electrochemical capacitance surface area measurements were used to estimate the number of active sites and the average activity of each site, as per-site turnover frequency (TOF)[44] (Figure SI9). The increase of the $\{Mo_3S_7\}_n$ loading (0.31−2.14 mg cm^{-2}) on the electrode increases the density of electrochemically accessible sites (~1.4 × 10^{16} to ~2.3 × 10^{17} sites cm^{-2}) giving TOF values for each active site between 1.00 and 0.42 s^{-1} at an overpotential of 0.2 V, which are in the same range as other amorphous molybdenum sulfides.[44] However, the $\{Mo_3S_4\}_n$ nanomaterial shows lower electrocatalytic accessible sites (~5.8 × 10^{15} to ~4.6 × 10^{17} sites cm^{-2}) yielding TOF between 0.31 and 0.05 s^{-1}.

The electrocatalytic HER activity of $\{Mo_3S_7\}_n$ increases by depositing a higher amount of this nanomaterial on the electrode (Figure 2a). Interestingly, with a 2.14 mg cm^{-2} catalyst loading resulting in a film thickness of around 0.35 μm on the glassy carbon RDE (see Figure SI10), a potential of −0.17 V vs RHE was required to reach a current density of 10 mA cm^{-2}, which is comparable with the state-of-the-art cluster-derived (Table SI1)[48−52,59] and amorphous molybdenum sulfide HER electrocatalysts (Table SI2).[31,38−44,46,47,59,78−84] However, a further increase in the catalyst loading does not enhance the catalytic performance.

The stability of $\{Mo_3S_7\}_n$ was assessed by cycling the material between 0.1 and −0.25 V vs RHE. After 500 cycles in H_2SO_4 0.5 M aqueous solution, the overpotential required to reach 10 mA cm^{-2} current density increases by only 15 mV, thus indicating a slight loss in HER activity (Figure 2b). Comparison of the high-resolution S 2p XPS core-level spectra of the pristine and the cycled catalyst (Figure 2c) revealed a decrease from 1.7 to 1.2, respectively, in the ratio of unsaturated bridging sulfur ligands (Mo_2-μ-S) to apical (Mo_3-μ_3-S) and saturated sulfurs linking different cluster units (Mo_2-μ−S-Mo). Moreover, the presence of a new band corresponding to physically adsorbed elemental S appeared in the XPS spectrum of the cycled catalyst. These results suggest that the unsaturated bridging sulfur ligands (Mo_2-μ-S) leach during the electrocatalytic performance and are deposited in form of inactive elemental S. Additionally, a discrete partial oxidation of the parent Mo^{IV} species to molybdenum oxysulfides ($Mo^yO_xS_y$) was also detected in the high-resolution Mo 3d core-level spectrum of the cycled catalyst (Figure 2d).[41] Although $\{Mo_3S_7\}_n$ experiences a slight deactivation, the overpotential required to reach a 10 mA cm^{-2} current density remains low.

Besides allowing access to amorphous molybdenum sulfides with activated basal planes, the use of molecular complexes as building entities provides an attractive strategy to freely engineer materials with atomic scale precision, investigate the self-assembly mechanism, and elucidate the nature of the active sites. Taking advantage of the isostructural character of the molybdenum chalcogenides complexes, the preparation of a broad diversity of nanomaterials based on $\{Mo_3Q_x\}_n$ (Q = S, Se; x = 4−7) extended structures was accomplished through the same bottom-up synthetic strategy as before, by using molecular complexes with Mo_3 (μ_3-S)(μ-S_{ax}-Se_{eq})$_3$, Mo_3(μ_3-S)(μ-Se_{ax}-Se_{eq})$_3$, Mo_3(μ_3-S)(μ-Se_{ax}-Se_{eq})$_3$, Mo_3(μ_3-Se)(μ-Se_{ax}-Se_{eq})$_3$, and Mo_3(μ_3-S)(μ-Se_{ax})$_3$ cluster cores (Figure 3a).

In particular, an accurate analysis of the sulfur and selenium 2p regions of the XPS spectra of the nanomaterials $\{Mo_3S_4Se_3\}_n$ and $\{Mo_3SSe_3S_3\}_n$, which are respectively obtained from the molecular sulfide clusters having selenium at the equatorial and axial positions, provides key insights to discern the ligands through which the self-assembly process takes place. This XPS region is dominated by two broad signals that were deconvoluted and fitted into several sets of doublets, characteristic of the spin−orbit splitting of the S and Se $2p_{3/2}$

https://doi.org/10.1021/acs.chemmater.3c01260
Chem. Mater. 2023, 35, 8483−8493

and $2p_{1/2}$ orbitals (Figure 3b,c, respectively). The assignment of the binding energies (BEs) was done according to the values previously set for the series of nanomaterials $\{Mo_3S_{4-7}\}_n$ and for the molecular cluster complexes containing the same type of Se species (Figures SI6, SI11, and SI12, Tables SI3 and SI4). Thus, two doublets located at BEs of 161.9/163.0 and 161.2/166.7 eV were assigned to unsaturated bridging S and Se ligands (Mo_2-μ-Q), respectively. The other two doublets centered at 162.6/163.8 eV for sulfur and 162.1/167.8 eV for selenium correspond to apical ligands (Mo_3-μ_3-Q) and to the saturated ones linking different cluster units (Mo_3-μ-Q-Mo). A detailed analysis of the relative areas of these doublets revealed that the self-assembly process takes place in a similar degree (around 25%) in both nanomaterials ($\{Mo_3S_4Se_3\}_n$ and $\{Mo_3SSe_3S_3\}_n$) with a preferential involvement (around 20%) of the species that originally were occupying the equatorial position in the molecular cluster precursors.

Next, the electrocatalytic HER properties of the obtained nanomaterials were investigated and further compared (Figure 3d). In general, the introduction of selenium species in the nanomaterial had a detrimental result. Therefore, $\{Mo_3S_7\}_n$ remained as the most active HER catalyst. A slight decrease in the activity, but still comparable, was observed by using the catalyst $\{Mo_3S_4Se_3\}_n$, which was obtained from the molecular cluster having Se at the equatorial positions. Notably, a more drastic decrease in the HER activity was sensed when the nanomaterials were derived from clusters in which the axial positions are occupied by Se, i.e., in the catalysts $\{Mo_3SSe_3S_4\}_n$, $\{Mo_3SSe_6\}_n$, and $\{Mo_3Se_7\}_n$. However, $\{Mo_3SSe_6\}_n$ and $\{Mo_3Se_7\}_n$ showed almost equal activity. All of these results suggest that the HER activity of these nanomaterials mainly originates from the unsaturated bridging chalcogenide ligands (Mo_2-μ-Q), which are generated upon the cluster self-assembly process and that originally occupied the axial positions, and to a lesser extent the equatorial ones, at the molecular cluster precursors. Moreover, saturated inter-cluster bridging chalcogenides (Mo_2-μ-Q-Mo), which mainly derive from equatorial cluster positions, are also active to some extent. On the contrary, the apical chalcogenides (Mo_3-μ_2-Q) scarcely influence the electrocatalytic performances. Incidentally, catalysts $\{Mo_3S_4\}_n$ and $\{Mo_3SSe_3\}_n$ showed the lowest activity, which can be ascribed to the lower density of unsaturated bridging chalcogenide ligands (Mo_2-μ-Q) in comparison with the nanomaterials $\{Mo_3Q_7\}_n$ (Q = S, Se).

Density functional theory (DFT) calculations were performed to further investigate the origin of the HER activity of the catalysts $\{Mo_3Q_{7-4}\}_n$ (Q = S, Se). The hydrogen adsorption free energy (ΔG_H) has been widely accepted as a good descriptor of HER activity for various electrocatalysts, the best performance being expected for systems with close to zero ΔG_H values.[10,85] At this point and following the Sabatier principle, hydrogen binds neither too strongly nor too weakly, resulting in the optimal HER electrocatalyst. Two trimer compositions were used to simulate the different configurations that the chalcogenide and molybdenum atoms can adopt into the prepared amorphous nanomaterials $\{Mo_3Q_{7-4}\}_n$ (Q = S, Se). In a first approximation, the trimer composition $Mo_9S_{12}O(OH)_{10}$, with one terminal Mo=O group and ten hydroxyl groups compensating the positive charges (Figure 4a), was used to model the nanomaterial $\{Mo_3S_4\}_n$. Apical (Mo_3-μ_3-S), unsaturated (Mo_2-μ-S), and saturated (Mo_2-μ-S-Mo) sulfur atoms can be found in this structural model. The calculated ΔG_H values (Table SI5 and Figure SI13), between

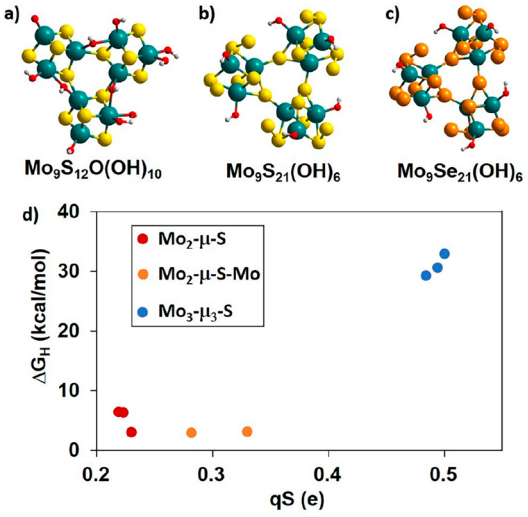

Figure 4. (a) $Mo_9S_{12}O(OH)_{10}$, (b) $Mo_9S_{21}(OH)_6$, and (c) $Mo_9Se_{21}(OH)_6$ trimers employed in DFT calculations. (d) Correlation between hydrogen adsorption free energy values ΔG_H in kcal/mol and net atomic charge on the S atoms in $Mo_9S_{21}(OH)_6$ trimers classified by type of S site.

26 and 35 kcal/mol for apical (Mo_3-μ_3-S) and lower than 5 kcal/mol for some unsaturated (Mo_2-μ-S) and saturated (Mo_2-μ-S-Mo) sulfur atoms, postulate these latter ones and rule out the apical ones as HER active sites. Additionally, coordinatively unsaturated molybdenum atoms, which were generated by removal of one hydroxyl group, were also considered. The low ΔG_H values obtained (ranging between −2.4 and 5.3 kcal/mol) suggest, in accordance with previously reported studies,[41] that coordination vacant sites around molybdenum atoms could also be feasible active sites for H_2 generation. To model the nanomaterial $\{Mo_3S_7\}_n$, we used a trimer of composition $Mo_9S_{21}(OH)_6$, in which, in order to preserve the charge neutrality, only one disulfide bond of each cluster unit was broken to form unsaturated (Mo_2-μ-S) and saturated (Mo_2-μ-S-Mo) sulfur atoms (Figure 4b). Again, H adsorption on apical (Mo_3-μ_3-S) sulfurs is the least favored, and for both unsaturated (Mo_2-μ-S) and saturated (Mo_2-μ−S-Mo) sulfur atoms, ΔG_H values close to 3 kcal/mol were found (Table SI5 and Figure SI14). Likewise, the Mo−H binding had a favorable result.

Further insights into the different activities of the sulfur species depending on their structural configuration (apical, unsaturated bridging, and saturated bridging) were obtained by inspection of their net atomic charge. As shown in Figure 4, the apical (Mo_3-μ_3-S) sulfurs, which display a higher positive charge, are less prone to stabilize hydrogen. The most favorable sulfur sites for the HER reaction (those with calculated ΔG_H close to zero) are the coordinatively unsaturated (Mo_2-μ-S) and saturated (Mo_2-μ-S-Mo) sulfur atoms. Importantly, slightly larger and therefore less favorable ΔG_H values were found when both models were built from molecular clusters containing Se atoms (Table SI5 and Figure SI15). The lower electronegativity of Se compared to S may lead to positions with higher positive charge, thus explaining the decrease in activity when Se is introduced in the different atomic positions.

https://doi.org/10.1021/acs.chemmater.3c01260
Chem. Mater. 2023, 35, 8483−8493

CONCLUSION

In conclusion, we have developed a cluster-based synthetic methodology to engineer amorphous molybdenum sulfide starting from Mo_3S_4 and Mo_3S_7 molecular cluster complexes, which allowed the introduction of active sites both at the naturally occurring edge positions and along the typically inactive basal planes. Derived from the extended-molecular nature of the obtained nanomaterials $\{Mo_3S_{4-7}\}_n$ and their processability in the form of heterojunction with conductive carbon supports, highly active HER electrocatalysts have been obtained. Fine chemical tuning in several atomic cluster positions was accomplished, allowing the generation of amorphous molybdenum sulfides with well-defined modifications with atomic-scale precision. This enabled us to track the synthesis mechanism, in which the cluster units preferentially condense through the sulfur atoms originally located at the equatorial positions of the molecular cluster complexes. Additionally, the combination of these experiments with DFT calculations shows that the active sites in these nanomaterials are the unsaturated intracluster (Mo_2-μ-S) and saturated intercluster (Mo_2-μ-S-Mo) bridging sulfur atoms, whereas the influence of the sulfurs in the apical position (Mo_3-μ_3-S) has been demonstrated to be negligible. Moreover, according to DFT calculations, unsaturated molybdenum atoms could also be active sites for the HER reaction. Nevertheless, the improvement in HER activity that occurred by increasing the sulfur/molybdenum ratio, in combination with the activity variation observed with the sulfur/selenium substitution experiments, fully suggests that the HER activity of these materials mainly arises from sulfur-derived species. This work shows how starting from well-defined cluster entities makes it possible to engineer highly active HER electrocatalysts and allows one to decipher the nature of the active sites, thus paving the way for the design or more efficient electrocatalytic materials.

ASSOCIATED CONTENT

Supporting Information

The Supporting Information is available free of charge at https://pubs.acs.org/doi/10.1021/acs.chemmater.3c01260.

Characterization of the molecular complexes, additional characterization of nanomaterials $\{Mo_3Q_{4-7}\}_n$ (Q = S, Se), extended data for HER electrocatalytic experiments, comparison of HER activity with state-of-the-art cluster-derived and amorphous molybdenum sulfides, and DFT data including hydrogen adsorption free energy (ΔG_H) values and optimized structures of hydrogen adsorption on different models (PDF)

AUTHOR INFORMATION

Corresponding Authors

Iván Sorribes − *Instituto de Tecnología Química, Universitat Politècnica de València-Consejo Superior de Investigaciones Científicas (UPV-CSIC), 46022 Valencia, Spain; Institute of Advanced Materials (INAM), Centro de Innovación en Química Avanzada (ORFEO-CINQA), Universitat Jaume I, 12006 Castellón, Spain;* orcid.org/0000-0002-3721-9335; Email: ivsorter@itq.upv.es, isorribe@uji.es

Avelino Corma − *Instituto de Tecnología Química, Universitat Politècnica de València-Consejo Superior de Investigaciones Científicas (UPV-CSIC), 46022 Valencia, Spain;* orcid.org/0000-0002-2232-3527; Email: acorma@itq.upv.es

Authors

Francisco Gonell − *Instituto de Tecnología Química, Universitat Politècnica de València-Consejo Superior de Investigaciones Científicas (UPV-CSIC), 46022 Valencia, Spain;* orcid.org/0000-0002-8658-2878

Miriam Rodenes − *Instituto de Tecnología Química, Universitat Politècnica de València-Consejo Superior de Investigaciones Científicas (UPV-CSIC), 46022 Valencia, Spain*

Santiago Martín − *Instituto de Nanociencia y Materiales de Aragón (INMA), CSIC, Universidad de Zaragoza, Zaragoza 50009, Spain;* orcid.org/0000-0001-9193-3874

Mercedes Boronat − *Instituto de Tecnología Química, Universitat Politècnica de València-Consejo Superior de Investigaciones Científicas (UPV-CSIC), 46022 Valencia, Spain;* orcid.org/0000-0002-6211-5888

Complete contact information is available at: https://pubs.acs.org/10.1021/acs.chemmater.3c01260

Notes

The authors declare no competing financial interest.

ACKNOWLEDGMENTS

This work has been supported by the Gen-T Plan of the Generalitat Valenciana through the programs "Subvencions a l'Excel·lència Científica de Jüniors Investigadors" (SEJI/2020/018) and "Investigadors Doctors d'Exel·lència" (CIDEXG/2022/22). Financial support by Severo Ochoa centre of excellence program (CEX2021-001230-S) is gratefully acknowledged. S.M. thanks DGA/fondos FEDER (construyendo Europa desde Aragón) for funding the research group Platon (E31_20R). M.R. and F.G. acknowledge the Vice-Rectorate for Research, Innovation and Transfer of the Universitat Politécnica de Valéncia (UPV) for a pre- and postdoctoral (PAID-10-20) fellowship, respectively. The authors also thank the Electron Microscopy Service of the UPV for TEM facilities and Dr. G. Antorrena for technical support in XPS studies.

REFERENCES

(1) Züttel, A.; Remhof, A.; Borgschulte, A.; Friedrichs, O. Hydrogen: The Future Energy Carrier. *Philos. Trans. R. Soc. A Math. Phys. Eng. Sci.* **2010**, *368* (1923), 3329−3342.

(2) He, T.; Pachfule, P.; Wu, H.; Xu, Q.; Chen, P. Hydrogen Carriers. *Nat. Rev. Mater.* **2016**, *1* (12), 16059.

(3) Greeley, J.; Jaramillo, T. F.; Bonde, J.; Chorkendorff, I.; Nørskov, J. K. Computational High-Throughput Screening of Electrocatalytic Materials for Hydrogen Evolution. *Nat. Mater.* **2006**, *5* (11), 909−913.

(4) Faber, M. S.; Jin, S. Earth-Abundant Inorganic Electrocatalysts and Their Nanostructures for Energy Conversion Applications. *Energy Environ. Sci.* **2014**, *7* (11), 3519−3542.

(5) Zeng, M.; Li, Y. Recent Advances in Heterogeneous Electrocatalysts for the Hydrogen Evolution Reaction. *J. Mater. Chem. A* **2015**, *3* (29), 14942−14962.

(6) Montoya, J. H.; Seitz, L. C.; Chakthranont, P.; Vojvodic, A.; Jaramillo, T. F.; Nørskov, J. K. Materials for Solar Fuels and Chemicals. *Nat. Mater.* **2017**, *16* (1), 70−81.

(7) Tributsch, H. Layer-Type Transition Metal Dichalcogenides - a New Class of Electrodes for Electrochemical Solar Cells. *Berichte der Bunsengesellschaft für Phys. Chemie* **1977**, *81* (4), 361−369.

(8) Tributsch, H.; Bennett, J. C. Electrochemistry and Photochemistry of MoS_2 Layer Crystals. I. *J. Electroanal. Chem. Interfacial Electrochem.* **1977**, *81* (1), 97−111.
(9) Hinnemann, B.; Moses, P. G.; Bonde, J.; Jørgensen, K. P.; Nielsen, J. H.; Horch, S.; Chorkendorff, I.; Nørskov, J. K. Biomimetic Hydrogen Evolution: MoS_2 Nanoparticles as Catalyst for Hydrogen Evolution. *J. Am. Chem. Soc.* **2005**, *127* (15), 5308−5309.
(10) Jaramillo, T. F.; Jørgensen, K. P.; Bonde, J.; Nielsen, J. H.; Horch, S.; Chorkendorff, I. Identification of Active Edge Sites for Electrochemical H_2 Evolution from MoS_2 Nanocatalysts. *Science.* **2007**, *317* (5834), 100−102.
(11) Lukowski, M. A.; Daniel, A. S.; Meng, F.; Forticaux, A.; Li, L.; Jin, S. Enhanced Hydrogen Evolution Catalysis from Chemically Exfoliated Metallic MoS_2 Nanosheets. *J. Am. Chem. Soc.* **2013**, *135* (28), 10274−10277.
(12) Chen, Z.; Cummins, D.; Reinecke, B. N.; Clark, E.; Sunkara, M. K.; Jaramillo, T. F. Core-Shell MoO_3 -MoS_2 Nanowires for Hydrogen Evolution: A Functional Design for Electrocatalytic Materials. *Nano Lett.* **2011**, *11* (10), 4168−4175.
(13) Kong, D.; Wang, H.; Cha, J. J.; Pasta, M.; Koski, K. J.; Yao, J.; Cui, Y. Synthesis of MoS_2 and $MoSe_2$ Films with Vertically Aligned Layers. *Nano Lett.* **2013**, *13* (3), 1341−1347.
(14) Kibsgaard, J.; Chen, Z.; Reinecke, B. N.; Jaramillo, T. F. Engineering the Surface Structure of MoS_2 To Preferentially Expose Active Edge Sites For Electrocatalysis. *Nat. Mater.* **2012**, *11* (11), 963−969.
(15) Li, Y.; Wang, H.; Xie, L.; Liang, Y.; Hong, G.; Dai, H. MoS_2 Nanoparticles Grown on Graphene: An Advanced Catalyst for the Hydrogen Evolution Reaction. *J. Am. Chem. Soc.* **2011**, *133* (19), 7296−7299.
(16) Li, D. J.; Maiti, U. N.; Lim, J.; Choi, D. S.; Lee, W. J.; Oh, Y.; Lee, G. Y.; Kim, S. O. Molybdenum Sulfide/N-Doped CNT Forest Hybrid Catalysts for High-Performance Hydrogen Evolution Reaction. *Nano Lett.* **2014**, *14* (3), 1228−1233.
(17) Liao, L.; Zhu, J.; Bian, X.; Zhu, L.; Scanlon, M. D.; Girault, H. H.; Liu, B. MoS_2 Formed on Mesoporous Graphene as a Highly Active Catalyst for Hydrogen Evolution. *Adv. Funct. Mater.* **2013**, *23* (42), 5326−5333.
(18) Zhang, X.; Jia, F.; Song, S. Recent Advances in Structural Engineering of Molybdenum Disulfide for Electrocatalytic Hydrogen Evolution Reaction. *Chem. Eng. J.* **2021**, *405*, 127013.
(19) Ye, G.; Gong, Y.; Lin, J.; Li, B.; He, Y.; Pantelides, S. T.; Zhou, W.; Vajtai, R.; Ajayan, P. M. Defects Engineered Monolayer MoS_2 for Improved Hydrogen Evolution Reaction. *Nano Lett.* **2016**, *16* (2), 1097−1103.
(20) Li, L.; Qin, Z.; Ries, L.; Hong, S.; Michel, T.; Yang, J.; Salameh, C.; Bechelany, M.; Miele, P.; Kaplan, D.; et al. Role of Sulfur Vacancies and Undercoordinated Mo Regions in MoS_2 Nanosheets toward the Evolution of Hydrogen. *ACS Nano* **2019**, *13* (6), 6824−6834.
(21) Kiriya, D.; Lobaccaro, P.; Nyein, H. Y. Y.; Taheri, P.; Hettick, M.; Shiraki, H.; Sutter-Fella, C. M.; Zhao, P.; Gao, W.; Maboudian, R.; et al. General Thermal Texturization Process of MoS_2 for Efficient Electrocatalytic Hydrogen Evolution Reaction. *Nano Lett.* **2016**, *16* (7), 4047−4053.
(22) Cheng, C.-C.; Lu, A.-Y.; Tseng, C.-C.; Yang, X.; Hedhili, M. N.; Chen, M.-C.; Wei, K.-H.; Li, L.-J. Activating Basal-Plane Catalytic Activity of Two-Dimensional MoS_2 Monolayer with Remote Hydrogen Plasma. *Nano Energy* **2016**, *30*, 846−852.
(23) Tao, L.; Duan, X.; Wang, C.; Duan, X.; Wang, S. Plasma-Engineered MoS_2 Thin-Film as an Efficient Electrocatalyst for Hydrogen Evolution Reaction. *Chem. Commun.* **2015**, *51* (35), 7470−7473.
(24) Yang, J.; Wang, Y.; Lagos, M. J.; Manichev, V.; Fullon, R.; Song, X.; Voiry, D.; Chakraborty, S.; Zhang, W.; Batson, P. E.; et al. Single Atomic Vacancy Catalysis. *ACS Nano* **2019**, *13* (9), 9958−9964.
(25) Kang, S.; Koo, J.-J.; Seo, H.; Truong, Q. T.; Park, J. B.; Park, S. C.; Jung, Y.; Cho, S.-P.; Nam, K. T.; Kim, Z. H.; et al. Defect-Engineered MoS_2 with Extended Photoluminescence Lifetime for High-Performance Hydrogen Evolution. *J. Mater. Chem. C* **2019**, *7* (33), 10173−10178.
(26) Zhang, P.; Xiang, H.; Tao, L.; Dong, H.; Zhou, Y.; Hu, T. S.; Chen, X.; Liu, S.; Wang, S.; Garaj, S. Chemically Activated MoS_2 for Efficient Hydrogen Production. *Nano Energy* **2019**, *57*, 535−541.
(27) Wang, X.; Zhang, Y.; Si, H.; Zhang, Q.; Wu, J.; Gao, L.; Wei, X.; Sun, Y.; Liao, Q.; Zhang, Z.; et al. Single-Atom Vacancy Defect to Trigger High-Efficiency Hydrogen Evolution of MoS_2. *J. Am. Chem. Soc.* **2020**, *142* (9), 4298−4308.
(28) Tsai, C.; Li, H.; Park, S.; Park, J.; Han, H. S.; Nørskov, J. K.; Zheng, X.; Abild-Pedersen, F. Electrochemical Generation of Sulfur Vacancies in the Basal Plane of MoS_2 for Hydrogen Evolution. *Nat. Commun.* **2017**, *8* (1), 15113.
(29) Deng, Y.; Liu, Z.; Wang, A.; Sun, D.; Chen, Y.; Yang, L.; Pang, J.; Li, H.; Li, H.; Liu, H.; et al. Oxygen-Incorporated MoX (X: S, Se or P) Nanosheets via Universal and Controlled Electrochemical Anodic Activation for Enhanced Hydrogen Evolution Activity. *Nano Energy* **2019**, *62* (May), 338−347.
(30) Deng, J.; Li, H.; Xiao, J.; Tu, Y.; Deng, D.; Yang, H.; Tian, H.; Li, J.; Ren, P.; Bao, X. Triggering the Electrocatalytic Hydrogen Evolution Activity of the Inert Two-Dimensional MoS_2 Surface via Single-Atom Metal Doping. *Energy Environ. Sci.* **2015**, *8* (5), 1594−1601.
(31) Merki, D.; Vrubel, H.; Rovelli, L.; Fierro, S.; Hu, X. Fe, Co, and Ni Ions Promote the Catalytic Activity of Amorphous Molybdenum Sulfide Films for Hydrogen Evolution. *Chem. Sci.* **2012**, *3* (8), 2515−2525.
(32) Lau, T. H. M.; Wu, S.; Kato, R.; Wu, T.-S.; Kulhavý, J.; Mo, J.; Zheng, J.; Foord, J. S.; Soo, Y.-L.; Suenaga, K.; et al. Engineering Monolayer 1T-MoS_2 into a Bifunctional Electrocatalyst via Sonochemical Doping of Isolated Transition Metal Atoms. *ACS Catal.* **2019**, *9* (8), 7527−7534.
(33) Geng, X.; Sun, W.; Wu, W.; Chen, B.; Al-Hilo, A.; Benamara, M.; Zhu, H.; Watanabe, F.; Cui, J.; Chen, T. Pure and Stable Metallic Phase Molybdenum Disulfide Nanosheets for Hydrogen Evolution Reaction. *Nat. Commun.* **2016**, *7* (1), 10672.
(34) Maitra, U.; Gupta, U.; De, M.; Datta, R.; Govindaraj, A.; Rao, C. N. R. Highly Effective Visible-Light-Induced H 2 Generation by Single-Layer 1T-MoS_2 and a Nanocomposite of Few-Layer 2H-MoS_2 with Heavily Nitrogenated Graphene. *Angew. Chemie Int. Ed.* **2013**, *52* (49), 13057−13061.
(35) Luo, Z.; Ouyang, Y.; Zhang, H.; Xiao, M.; Ge, J.; Jiang, Z.; Wang, J.; Tang, D.; Cao, X.; Liu, C.; et al. Chemically Activating MoS_2 via Spontaneous Atomic Palladium Interfacial Doping towards Efficient Hydrogen Evolution. *Nat. Commun.* **2018**, *9* (1), 2120.
(36) Voiry, D.; Yamaguchi, H.; Li, J.; Silva, R.; Alves, D. C. B.; Fujita, T.; Chen, M.; Asefa, T.; Shenoy, V. B.; Eda, G.; et al. Enhanced Catalytic Activity in Strained Chemically Exfoliated WS_2 Nanosheets for Hydrogen Evolution. *Nat. Mater.* **2013**, *12* (9), 850−855.
(37) Solati, N.; Karakaya, C.; Kaya, S. Advancing the Understanding of the Structure-Activity-Durability Relation of 2D MoS_2 for the Hydrogen Evolution Reaction. *ACS Catal.* **2023**, *13* (1), 342−354.
(38) Vrubel, H.; Hu, X. Growth and Activation of an Amorphous Molybdenum Sulfide Hydrogen Evolving Catalyst. *ACS Catal.* **2013**, *3* (9), 2002−2011.
(39) Mabayoje, O.; Liu, Y.; Wang, M.; Shoola, A.; Ebrahim, A. M.; Frenkel, A. I.; Mullins, C. B. Electrodeposition of MoS_x Hydrogen Evolution Catalysts from Sulfur-Rich Precursors. *ACS Appl. Mater. Interfaces* **2019**, *11* (36), 32879−32886.
(40) Lassalle-Kaiser, B.; Merki, D.; Vrubel, H.; Gul, S.; Yachandra, V. K.; Hu, X.; Yano, J. Evidence from in Situ X-Ray Absorption Spectroscopy for the Involvement of Terminal Disulfide in the Reduction of Protons by an Amorphous Molybdenum Sulfide Electrocatalyst. *J. Am. Chem. Soc.* **2015**, *137* (1), 314−321.
(41) Tran, P. D.; Tran, T. V.; Orio, M.; Torelli, S.; Truong, Q. D.; Nayuki, K.; Sasaki, Y.; Chiam, S. Y.; Yi, R.; Honma, I.; et al. Coordination Polymer Structure and Revisited Hydrogen Evolution Catalytic Mechanism for Amorphous Molybdenum Sulfide. *Nat. Mater.* **2016**, *15* (6), 640−646.

https://doi.org/10.1021/acs.chemmater.3c01260
Chem. Mater. 2023, 35, 8483−8493

(42) Deng, Y.; Ting, L. R. L.; Neo, P. H. L.; Zhang, Y.-J.; Peterson, A. A.; Yeo, B. S. Operando Raman Spectroscopy of Amorphous Molybdenum Sulfide (MoS_x) during the Electrochemical Hydrogen Evolution Reaction: Identification of Sulfur Atoms as Catalytically Active Sites for H^+ Reduction. *ACS Catal.* **2016**, *6* (11), 7790−7798.
(43) Ting, L. R. L.; Deng, Y.; Ma, L.; Zhang, Y.-J.; Peterson, A. A.; Yeo, B. S. Catalytic Activities of Sulfur Atoms in Amorphous Molybdenum Sulfide for the Electrochemical Hydrogen Evolution Reaction. *ACS Catal.* **2016**, *6* (2), 861−867.
(44) Benck, J. D.; Chen, Z.; Kuritzky, L. Y.; Forman, A. J.; Jaramillo, T. F. Amorphous Molybdenum Sulfide Catalysts for Electrochemical Hydrogen Production: Insights into the Origin of Their Catalytic Activity. *ACS Catal.* **2012**, *2* (9), 1916−1923.
(45) Vrubel, H.; Merki, D.; Hu, X. Hydrogen Evolution Catalyzed by MoS_3 and MoS_2 Particles. *Energy Environ. Sci.* **2012**, *5* (3), 6136.
(46) Chang, Y.-H.; Lin, C.-T.; Chen, T.-Y.; Hsu, C.-L.; Lee, Y.-H.; Zhang, W.; Wei, K.-H.; Li, L.-J. Highly Efficient Electrocatalytic Hydrogen Production by MoS_x Grown on Graphene-Protected 3D Ni Foams. *Adv. Mater.* **2013**, *25* (5), 756−760.
(47) Casalongue, H. G. S.; Benck, J. D.; Tsai, C.; Karlsson, R. K. B.; Kaya, S.; Ng, M. L.; Pettersson, L. G. M.; Abild-Pedersen, F.; Nørskov, J. K.; Ogasawara, H.; et al. Operando Characterization of an Amorphous Molybdenum Sulfide Nanoparticle Catalyst during the Hydrogen Evolution Reaction. *J. Phys. Chem. C* **2014**, *118* (50), 29252−29259.
(48) Jaramillo, T. F.; Bonde, J.; Zhang, J.; Ooi, B.-L.; Andersson, K.; Ulstrup, J.; Chorkendorff, I. Hydrogen Evolution on Supported Incomplete Cubane-Type $[Mo_3S_4]^{4+}$ Electrocatalysts. *J. Phys. Chem. C* **2008**, *112* (45), 17492−17498.
(49) Kibsgaard, J.; Jaramillo, T. F.; Besenbacher, F. Building an Appropriate Active-Site Motif into a Hydrogen-Evolution Catalyst with Thiomolybdate $[Mo_3S_{13}]^{2-}$ Clusters. *Nat. Chem.* **2014**, *6* (3), 248−253.
(50) Shang, Y.; Xu, X.; Gao, B.; Ren, Z. Thiomolybdate $[Mo_3S_{13}]^{2-}$ Nanoclusters Anchored on Reduced Graphene Oxide-Carbon Nanotube Aerogels for Efficient Electrocatalytic Hydrogen Evolution. *ACS Sustain. Chem. Eng.* **2017**, *5* (10), 8908−8917.
(51) Ji, Z.; Trickett, C.; Pei, X.; Yaghi, O. M. Linking Molybdenum-Sulfur Clusters for Electrocatalytic Hydrogen Evolution. *J. Am. Chem. Soc.* **2018**, *140* (42), 13618−13622.
(52) Du, K.; Zheng, L.; Wang, T.; Zhuo, J.; Zhu, Z.; Shao, Y.; Li, M. Electrodeposited Mo_3S_{13} Films from $(NH_4)_2Mo_3S_{13}{\cdot}2H_2O$ for Electrocatalysis of Hydrogen Evolution Reaction. *ACS Appl. Mater. Interfaces* **2017**, *9* (22), 18675−18681.
(53) Hou, Y.; Abrams, B. L.; Vesborg, P. C. K.; Björketun, M. E.; Herbst, K.; Bech, L.; Setti, A. M.; Damsgaard, C. D.; Pedersen, T.; Hansen, O.; et al. Bioinspired Molecular Co-Catalysts Bonded to a Silicon Photocathode for Solar Hydrogen Evolution. *Nat. Mater.* **2011**, *10* (6), 434−438.
(54) Seo, S. W.; Park, S.; Jeong, H.-Y.; Kim, S. H.; Sim, U.; Lee, C. W.; Nam, K. T.; Hong, K. S. Enhanced Performance of $NaTaO_3$ Using Molecular Co-Catalyst $[Mo_3S_4]^{4+}$ for Water Splitting into H_2 and O_2. *Chem. Commun.* **2012**, *48* (84), 10452.
(55) Recatalá, D.; Llusar, R.; Gushchin, A. L.; Kozlova, E. A.; Laricheva, Y. A.; Abramov, P. A.; Sokolov, M. N.; Gómez, R.; Lana-Villarreal, T. Photogeneration of Hydrogen from Water by Hybrid Molybdenum Sulfide Clusters Immobilized on Titania. *ChemSusChem* **2015**, *8* (1), 148−157.
(56) Kan, M.; Jia, J.; Zhao, Y. High Performance Nanoporous Silicon Photoelectrodes Co-Catalyzed with an Earth Abundant $[Mo_3S_{13}]^{2-}$ Nanocluster via Drop Coating. *RSC Adv.* **2016**, *6* (19), 15610−15614.
(57) Dave, M.; Rajagopal, A.; Damm-Ruttensperger, M.; Schwarz, B.; Nägele, F.; Daccache, L.; Fantauzzi, D.; Jacob, T.; Streb, C. Understanding Homogeneous Hydrogen Evolution Reactivity and Deactivation Pathways of Molecular Molybdenum Sulfide Catalysts. *Sustain. Energy Fuels* **2018**, *2* (5), 1020−1026.
(58) Hou, Y. Photoelectrocatalysis and Electrocatalysis on Silicon Electrodes Decorated with Cubane-like Clusters. *J. Photonics Energy* **2012**, *2* (1), 026001.
(59) Seo, B.; Jung, G. Y.; Lee, S. J.; Baek, D. S.; Sa, Y. J.; Ban, H. W.; Son, J. S.; Park, K.; Kwak, S. K.; Joo, S. H. Monomeric MoS_4^{2-}-Derived Polymeric Chains with Active Molecular Units for Efficient Hydrogen Evolution Reaction. *ACS Catal.* **2020**, *10* (1), 652−662.
(60) Rodenes, M.; Gonell, F.; Martín, S.; Corma, A.; Sorribes, I. Molecularly Engineering Defective Basal Planes in Molybdenum Sulfide for the Direct Synthesis of Benzimidazoles by Reductive Coupling of Dinitroarenes with Aldehydes. *JACS Au* **2022**, *2* (3), 601−612.
(61) Fedin, V. P.; Sokolov, M. N.; Mironov, Y. V.; Kolesov, B. A.; Tkachev, S. V.; Fedorov, V. Y. Triangular Thiocomplexes of Molybdenum: Reactions with Halogens, Hydrohalogen Acids and Phosphines. *Inorg. Chim. Acta* **1990**, *167* (1), 39−45.
(62) Fedin, V. P.; Mironov, Y. V.; Sokolov, M. N.; Kolesov, B. A.; Federov, V. Y.; Yufit, D. S.; Struchkov, Y. T. Synthesis, Structure, Vibrational Spectra and Chemical Properties of the Triangular Molybdenum and Tungsten Complexes M_3 (μ_3-S)(μ_2-SSe)$_3X_6^{2-}$ (M = Mo, W; X = Cl, Br). *Inorg. Chim. Acta* **1990**, *174* (2), 275−282.
(63) Saysell, D. M.; Fedin, V. P.; Lamprecht, G. J.; Sokolov, M. N.; Sykes, A. G. Preparation and Solution Properties of Chalcogenide-Rich Clusters $[Mo_3Y_7(H_2O)_6]^{4+}$ (Y = S, Se): Kinetics of PR_3^{3-} Abstraction of Y from μ-(Y_2^{2-}) and H_2O Substitution by Cl^- and Br^-. *Inorg. Chem.* **1997**, *36* (14), 2982−2987.
(64) Hernandez-Molina, R.; Dybtsev, D. N.; Fedin, V. P.; Elsegood, M. R. J.; Clegg, W.; Sykes, A. G. Preparation, Structure, and Reactivity of Heterometallic Sn-Containing Single- and Double-Cube Derivatives of $[Mo_3Se_4(H_2O)_9]^{4+}$ and $[W_3Se_4(H_2O)_9]^{4+}$. *Inorg. Chem.* **1998**, *37* (12), 2995−3001.
(65) Gushchin, A. L.; Ooi, B.-L.; Harris, P.; Vicent, C.; Sokolov, M. N. Synthesis and Characterization of Mixed Chalcogen Triangular Complexes with New Mo_3 (μ_3-S)(μ_2-Se$_2$)$_3^{4+}$ and M_3 (μ_3-S)(μ_2-Se)$_3^{4+}$ (M = Mo, W) Cluster Cores. *Inorg. Chem.* **2009**, *48* (8), 3832−3839.
(66) Hernández-Molina, R.; Sokolov, M.; Núñez, P.; Mederos, A. Synthesis and Structure of $[M_3(\mu_3\text{-Se})(\mu\text{-SeS})_3]^{4+}$ Core Compounds (M = Mo, W): A Less-Common Type of Linkage Isomerism for the μ-SSe Ligand. *J. Chem. Soc. Dalt. Trans.* **2002**, *3* (6), 1072−1077.
(67) Frisch, M. J.; Trucks, G. W.; Schlegel, H. B.; Scuseria, G. E.; Robb, M. A.; Cheeseman, J. R.; Scalmani, G.; Barone, V.; Petersson, G. A.; Nakatsuji, H.; et al. *Gaussian 09*, Rev. D.01; Gaussian Inc.: Wallingford, CT, 2016.
(68) Becke, A. D. Density-functional Thermochemistry. III. The Role of Exact Exchange. *J. Chem. Phys.* **1993**, *98* (7), 5648−5652.
(69) Lee, C.; Yang, W.; Parr, R. G. Development of the Colle-Salvetti Correlation-Energy Formula into a Functional of the Electron Density. *Phys. Rev. B* **1988**, *37* (2), 785−789.
(70) McLean, A. D.; Chandler, G. S. Contracted Gaussian Basis Sets for Molecular Calculations. I. Second Row Atoms, Z = 11−18. *J. Chem. Phys.* **1980**, *72* (10), 5639−5648.
(71) Curtiss, L. A.; McGrath, M. P.; Blaudeau, J.; Davis, N. E.; Binning, R. C.; Radom, L. Extension of Gaussian-2 Theory to Molecules Containing Third-row Atoms Ga-Kr. *J. Chem. Phys.* **1995**, *103* (14), 6104−6113.
(72) Hay, P. J.; Wadt, W. R. Ab Initio Effective Core Potentials for Molecular Calculations. Potentials for the Transition Metal Atoms Sc to Hg. *J. Chem. Phys.* **1985**, *82* (1), 270−283.
(73) Hay, P. J.; Wadt, W. R. Ab Initio Effective Core Potentials for Molecular Calculations. Potentials for K to Au Including the Outermost Core Orbitals. *J. Chem. Phys.* **1985**, *82* (1), 299−310.
(74) Reed, A. E.; Weinstock, R. B.; Weinhold, F. Natural Population Analysis. *J. Chem. Phys.* **1985**, *83* (2), 735−746.
(75) Rodenes, M.; Dhaeyere, F.; Martín, S.; Concepción, P.; Corma, A.; Sorribes, I. Multifunctional Catalysis of Nanosheet Defective Molybdenum Sulfide Basal Planes for Tandem Reactions Involving Alcohols and Molecular Hydrogen. *ACS Sustainable Chem. Eng.* **2023**, *11* (33), 12265−12279.
(76) Sorribes, I.; Liu, L.; Corma, A. Nanolayered Co-Mo-S Catalysts for the Chemoselective Hydrogenation of Nitroarenes. *ACS Catal.* **2017**, *7* (4), 2698−2708.

https://doi.org/10.1021/acs.chemmater.3c01260
Chem. Mater. 2023, 35, 8483−8493

(77) Xi, F.; Bogdanoff, P.; Harbauer, K.; Plate, P.; Höhn, C.; Rappich, J.; Wang, B.; Han, X.; van de Krol, R.; Fiechter, S. Structural Transformation Identification of Sputtered Amorphous MoS x as an Efficient Hydrogen-Evolving Catalyst during Electrochemical Activation. *ACS Catal.* **2019**, *9* (3), 2368−2380.
(78) Lee, C.-H.; Lee, S.; Kang, G.-S.; Lee, Y.-K.; Park, G. G.; Lee, D. C.; Joh, H.-I. Insight into the Superior Activity of Bridging Sulfur-Rich Amorphous Molybdenum Sulfide for Electrochemical Hydrogen Evolution Reaction. *Appl. Catal. B Environ.* **2019**, *258*, 117995.
(79) Ye, Z.; Yang, J.; Li, B.; Shi, L.; Ji, H.; Song, L.; Xu, H. Amorphous Molybdenum Sulfide/Carbon Nanotubes Hybrid Nanospheres Prepared by Ultrasonic Spray Pyrolysis for Electrocatalytic Hydrogen Evolution. *Small* **2017**, *13* (21), 1700111.
(80) Ding, R.; Wang, M.; Wang, X.; Wang, H.; Wang, L.; Mu, Y.; Lv, B. N-Doped Amorphous MoS_x for the Hydrogen Evolution Reaction. *Nanoscale* **2019**, *11* (23), 11217−11226.
(81) Wang, D.; Li, H.; Du, N.; Hou, W. Amorphous Molybdenum Sulfide Monolayer Nanosheets for Highly Efficient Electrocatalytic Hydrogen Evolution. *Chem. Eng. J.* **2020**, *398*, 125685.
(82) Merki, D.; Fierro, S.; Vrubel, H.; Hu, X. Amorphous Molybdenum Sulfide Films as Catalysts for Electrochemical Hydrogen Production in Water. *Chem. Sci.* **2011**, *2* (7), 1262−1267.
(83) Benck, J. D.; Hellstern, T. R.; Kibsgaard, J.; Chakthranont, P.; Jaramillo, T. F. Catalyzing the Hydrogen Evolution Reaction (HER) with Molybdenum Sulfide Nanomaterials. *ACS Catal.* **2014**, *4* (11), 3957−3971.
(84) Aslan, E.; Yanalak, G.; Patir, I. H. Enhanced Hydrogen Evolution Reaction Catalysis at Template-Free Liquid/Liquid Interfaces by *In Situ* Electrodeposited Amorphous Molybdenum Sulfide on Carbon Nanotubes. *ACS Appl. Energy Mater.* **2021**, *4*, 8330−8339.
(85) Nørskov, J. K.; Bligaard, T.; Logadottir, A.; Kitchin, J. R.; Chen, J. G.; Pandelov, S.; Stimming, U. Trends in the Exchange Current for Hydrogen Evolution. *J. Electrochem. Soc.* **2005**, *152* (3), J23.

https://doi.org/10.1021/acs.chemmater.3c01260
Chem. Mater. 2023, 35, 8483−8493